



# CHORUS

This is the accepted manuscript made available via CHORUS. The article has been published as:

## Numerical analysis of electroconvection in cross-flow with unipolar charge injection

Yifei Guan and Igor Novosselov

Phys. Rev. Fluids **4**, 103701 — Published 1 October 2019

DOI: [10.1103/PhysRevFluids.4.103701](https://doi.org/10.1103/PhysRevFluids.4.103701)

# Numerical Analysis of Electroconvection in Cross-flow with Unipolar Charge Injection

Yifei Guan<sup>1</sup> and Igor Novosselov<sup>1,2, §</sup>

<sup>1</sup>*Department of Mechanical Engineering, University of Washington, Seattle, U.S.A. 98195*

<sup>2</sup>*Institute for Nano-Engineered Systems, University of Washington, Seattle, U.S.A. 98195*

January 2019

Electroconvection driven by unipolar charge injection in the presence of cross-flow between two parallel electrodes is investigated in a numerical study. The two-relaxation-time Lattice Boltzmann Method with fast Poisson solver is used to resolve the spatiotemporal distribution of flow field, electric field, and charge density. Couette and Poiseuille cross-flows are applied to the solutions with established electroconvective vortices. Increasing cross-flow velocity deforms the vortices and eventually suppresses them when threshold values of velocities are reached. At intermediate flow velocities, partial suppression of the vortices leads to the reduction in electroconvection. This behavior is parameterized by a non-dimensional parameter,  $Y$  — a ratio of the electrical forcing term to the viscous term in the Navier-Stokes Equations. For high values of  $Y$ , the electric force dominates the flow, while for values below the critical threshold, the electric force influence is negligible, and the flow is dominated by the shear.

## I. INTRODUCTION

Electroconvection (EC) phenomenon has been first reported by G. I. Taylor in 1966 describing cellular convection in the liquid droplet [1]. Since then, EC has been observed in a number of systems where the interaction of electrostatic force with fluids is present. In nonequilibrium electrohydrodynamic (EHD) systems [1-22], poorly conductive leaky dielectric fluid acquire unipolar charge injection at the surface interface in response to the electric field. Charge transport in the fluid can trigger instabilities leading to the development of EC vortices [23,24]. In charge-neutral electrokinetic (EK) systems, electroconvection is triggered by the electro-osmotic slip of electrolyte in the electric double layer at membrane surfaces [25-36].

Insights into the complex multiphysics interactions are essential for understanding EK and EHD phenomena. These include (1) the electric field from the potential difference between the anode and cathode and its modifications by the space charge effects; (2) the ion motion in the electric field; (3) the interaction between the motion of ions and the neutral molecules; and (4) the inertial and viscous forces in the complex flow. The EHD was used to describe the cellular convection in deforming oil droplet under a DC electric field [1], and droplet generation in microfluidic flow and oil separation [1,24,37]. The EC vortices have been observed in the systems where convective transport is induced by unipolar discharge into a dielectric fluid [2-22]. The model system describing EHD electroconvection is also known as the Taylor-Melcher (TM) model. The experiment demonstrating the electroconvective flow in the system with unipolar charge injection was first reported by Jolly & Melcher in 1970 [2] and by Watson and Schneider in the same year [38]. Jolly & Melcher had found that the incipient cellular convection can be characterized by the electric Hartmann number  $Ha_e = \varepsilon E / \sqrt{\mu\sigma}$  ( $\varepsilon$ -permittivity,  $E$ -applied electric field intensity,  $\mu$ -

---

<sup>§</sup> ivn@uw.edu

45 viscosity,  $\sigma$ -electric conductivity) with the assumption of uniform charge density in the fluids  
46 [2]. Watson and Schneider performed experiments on EHD stability in a space-charge-limit  
47 (SCL) current injection and found that there is a transition between SCL conduction and  
48 convection-enhanced conduction marked by the increased conductivity due to the motion of  
49 the fluids [38]. Atten et al. have shown that for the SCL scenario  $T_c = 100$ , where  $T_c$  is the  
50 linear stability threshold for the electric Rayleigh number  $T$ — a ratio between electric force  
51 to the viscous force [13,18,39,40]. The parameter  $T$  is also sometimes referred to as electric  
52 Taylor number [18], thus denoted as  $T$ . The chaotic behavior of EC instabilities was  
53 investigated experimentally by Malraison & Atten, who characterized two types of power  
54 spectra of intensity fluctuations, i.e., an exponential decay when viscous force is dominant  
55 and a power-law decay when inertial force is dominant [3]. The EC coupled to heat transfer  
56 was first experimentally shown by Atten et al., who observed that the Nusselt number (Nu)  
57 depends on applied electric field intensity [41]. In the annulus between concentric circular  
58 electrodes, the electric Nusselt number (Ne) trend can be described by the power-law  
59 function of electric Rayleigh number and electric Prandtl number [7,8].

60 The analysis of EC stability was first performed using a simplified non-linear  
61 hydraulic model [42,43] and linear stability analysis without charge diffusion [38,44]. Atten  
62 & Moreau [45] showed that in the weak-injection limit,  $C \ll 1$ , where  $C$  is the charge  
63 injection level, the flow stability is determined by the criterion  $T_c C^2$ . In the SCL injection,  
64  $C \rightarrow \infty$ , the flow stability is determined by  $T_c$  only. Non-linear stability analysis yields  
65  $T_c = 160.75$  [46], while the experiments yield  $T_c = 100$  for the same conditions [47]. Atten et al.  
66 suggested that the discrepancy may be due to the omission of the charge diffusion term in the  
67 analysis [46,48]. The effect of charge diffusion was investigated by Zhang et al. by  
68 employing linear stability analysis with a Poiseuille flow [13] and by non-linear analysis  
69 using a multiscale method [18]. The authors found that the charge diffusion has a non-  
70 negligible effect on  $T_c$  and the transient behavior depends on the Reynolds number ( $Re$ )  
71 [13,18]. More recently, Li et al. performed linear analysis of EHD-Poiseuille system and  
72 found that when the ratio of Coulomb force to viscous force increases, the transverse rolls can  
73 transition from convective instability to absolute instability [49]. Even with the inclusion of  
74 charge diffusion in the linear and non-linear stability analysis, the predicted stability criterion  
75  $T_c$  is always greater than the experimental value obtained by Lacroix et al. [47] and Atten et  
76 al. [46]. Lacroix et al. attributed this discrepancy to the instability associated with finite  
77 perturbation [47] suggesting that the experimental instability resulted from small perturbation  
78 (disturbance due to imperfection or error) and the theoretical solutions developed from  
79 applied finite-amplitude perturbation [47].

80 In the charge-neutral EK system, Rubinstein and Zaltzman showed that the electro-  
81 osmotic slip at the surface leading to instability of the double layer generating EC paired  
82 vortices; thus enhancing ion exchange at the membrane surface [25-27]. Demekhin et al. [50]  
83 modeled electrokinetic instability (EKI) decoupling the nonlinear Poisson-Nernst-Planck  
84 (PNP) equations and neglecting the inertial term in the Navier-Stokes equations (NSE). Pham  
85 et al. [29] performed direct numerical simulation (DNS) demonstrating that the charge-  
86 neutral EKI system exhibits a hysteretic behavior in the transition between the limiting and  
87 overlimiting regimes. Kwak et al. [30] have examined the effect of the cross-flow on the EKI  
88 and proposed a scaling law relating the field strength and shear to the height of the vortices.  
89 More recently, Kwak et al. extended the scaling law analysis for the electric Nusselt number  
90 as a function of the electric Rayleigh and Reynolds numbers for the EC-induced convective  
91 ion transport [31].

92 The EC stability problems in both EK and EHD systems were shown to be analogous  
93 to Rayleigh-Bernard convection (RBC) [22,51-58]. Of particular interest to this work is the  
94 suppression of the RBC cells in the cross-flow [59]. Richardson number  $Ri = Gr / Re^2$ , the  
95 ratio of buoyancy to the inertia force, has been used to parametrize the effect of the applied  
96 shear, where  $Gr$  is the Grashof number. For  $Ri > 10$ , the effect of the cross-flow is  
97 insignificant, while for  $Ri < 0.1$ , the effect of the buoyancy can be neglected. In the EC  
98 scenario, 2D finite volume simulations of Poiseuille flow show that the critical electric  
99 Rayleigh number,  $T_c$ , depends on the  $Re$  and ion mobility parameter,  $M$  [14]. The model for  
100 the EC system is more complicated than the RBC due to the introduction of two independent  
101 variables, i.e., the charge density and electric field. With the Boussinesq approximation, the  
102 RBC system is a two-way coupling of fluids motion and heat [60], on the other hand, EC is a  
103 three-way coupling between fluids, charge density, and electric field.

104 To gain insight into the complexity of the EC flow, the problem can be investigated  
105 using numerical simulations. The earlier finite-difference simulations have shown that strong  
106 numerical diffusivity may contaminate the model [4]. Other numerical approaches include the  
107 particle-in-cell method [61], finite volume method with the flux-corrected transport scheme  
108 [62], total variation diminishing scheme [9,11,15-17], and the method of characteristics [6].  
109 Luo et al. showed that a Lattice Boltzmann model (LBM) could predict the linear and finite-  
110 amplitude stability criteria of the subcritical bifurcation [19-22] for both 2D and 3D EC flow  
111 scenarios. This unified LBM transforms the elliptic Poisson equation to a parabolic  
112 advection-diffusion equation and introduces tuning coefficients to control the evolution of the  
113 electric potential, requiring additional sub-iterations at each time step.

114 Researching the interaction between EHD-driven EC instabilities and the external  
115 flow, Castellanos et al. performed a linear stability analysis of Poiseuille and Couette flow  
116 under unipolar injection. The authors showed that the external flow inhibits the transverse  
117 perturbation, but the longitudinal rolls remain unaffected [63]. Lara et al. found that the  
118 stability of traverse rolls depends on the mobility ratio  $M$  (Eq. (9)) in the low Reynolds  
119 number Poiseuille flow by performing linear stability analysis [64]. The current paper  
120 investigates the effects of crossflow on EC convection in unipolar charge injection scenario  
121 numerically.

122 In this paper, we parameterize the 2D EC stability in the cross-flow between two  
123 parallel electrodes in the presence of strong unipolar injection and electric field. The  
124 segregated solver combines a two-relaxation-time (TRT) LBM modeling fluid and charged  
125 species transport, and a Fast Fourier Transform Poisson solver to solve for the electric field  
126 directly [65]. Couette and Poiseuille cross-flow scenarios provide shear stress; the dominant  
127 terms are determined by non-dimensional analysis of the governing equations. A subcritical  
128 bifurcation is characterized by the ratio of the electrical force to the viscous force.

## 129 II. GOVERNING EQUATIONS AND DIMENSIONAL ANALYSIS

130 The governing equations for EHD flow include the Navier-Stokes equations (NSE)  
131 with the electric forcing term  $\mathbf{F}_e = -\rho_c \nabla \varphi$  in the momentum equation, the charge transport  
132 equation, and the Poisson equation for electric potential. The TM model describes cellular  
133 convection driven by unipolar charge injection for fluids with constant dielectric, and it can  
134 be parameterized in terms of non-dimensional parameters[11-17,19-22,49,66].

135 
$$\nabla \cdot \mathbf{u} = 0, \quad (1)$$

136 
$$\rho \frac{D\mathbf{u}}{Dt} = -\nabla P + \mu \nabla^2 \mathbf{u} - \rho_c \nabla \varphi, \quad (2)$$

137 
$$\frac{\partial \rho_c}{\partial t} + \nabla \cdot [(\mathbf{u} - \mu_b \nabla \varphi) \rho_c - D_c \nabla \rho_c] = 0, \quad (3)$$

138 
$$\nabla^2 \varphi = -\frac{\rho_c}{\varepsilon}, \quad (4)$$

139 where  $\rho$  and  $\mu$  are the density and the dynamic viscosity of the working fluid,  $\mathbf{u} = (u_x, u_y)$  is  
 140 the velocity vector field,  $P$  is the static pressure,  $\mu_b$  is the ion mobility,  $D_c$  is the ion  
 141 diffusivity,  $\rho_c$  is the charge density,  $\varepsilon$  is the electric permittivity, and  $\varphi$  is the electric  
 142 potential. The electric force provides a source term in the momentum equation (Eq. (2))  
 143 [13,67-69]. The variables to be solved are the velocity field --  $\mathbf{u}$ , pressure --  $P$ , charge  
 144 density --  $\rho_c$ , and electric potential --  $\varphi$ . The flow is modeled as periodic in the horizontal  
 145 direction (x-direction), and wall-bounded in the y-direction. Cross-flow is applied in the x-  
 146 direction.

147 In the absence of cross-flow, the system can be non-dimensionalized with the electric  
 148 field properties alone [13], i.e.,  $H$  is the distance between the electrodes (two plates infinite in  
 149 x and y),  $\rho_0$  is the injected charge density at the anode, and  $\Delta\varphi_0$  is the voltage difference  
 150 applied to the electrodes. Respectively, the time  $t$  is non-dimensionalized by  $H^2 / (\mu_b \Delta\varphi_0)$ ,  
 151 the velocity  $\mathbf{u}$  by the ion drift velocity  $u_{drift} = \mu_b \Delta\varphi_0 / H$ , the pressure  $P$  by  $\rho_0 (\mu_b \Delta\varphi_0)^2 / H^2$ ,  
 152 and the charge density in the domain  $\rho_c$  by  $\rho_0$ . Therefore, a non-dimensional form of the  
 153 governing equations (Eq. (1)-(4)) is:

154 
$$\nabla^* \cdot \mathbf{u}^* = 0, \quad (5)$$

155 
$$\frac{D^* \mathbf{u}^*}{D^* t^*} = -\nabla^* P^* + \frac{M^2}{T} \nabla^{*2} \mathbf{u}^* - C M^2 \rho_c^* \nabla^* \varphi^*, \quad (6)$$

156 
$$\frac{\partial^* \rho_c^*}{\partial^* t^*} + \nabla^* \cdot [(\mathbf{u}^* - \nabla^* \varphi^*) \rho_c^* - \frac{1}{Fe} \nabla^* \rho_c^*] = 0, \quad (7)$$

157 
$$\nabla^{*2} \varphi^* = -C \rho_c^*, \quad (8)$$

158 where the asterisk denotes the non-dimensional variables. These non-dimensional governing  
 159 equations yield four dimensionless parameters describing the system's state [9-22].

160 
$$M = \frac{(\varepsilon / \rho)^{1/2}}{\mu_b}, \quad T = \frac{\varepsilon \Delta\varphi_0}{\mu \mu_b}, \quad C = \frac{\rho_0 H^2}{\varepsilon \Delta\varphi_0}, \quad Fe = \frac{\mu_b \Delta\varphi_0}{D_e}, \quad (9)$$

161 The physical interpretations of these parameters are as follows:  $M$  is the ratio between  
 162 hydrodynamic mobility and the ionic mobility;  $T$  is the ratio between electric force to the  
 163 viscous force;  $C$  is the charge injection level [13,18]; and  $Fe$  is the reciprocal of the charge  
 164 diffusivity coefficient [13,18].

165 With the addition of a cross-flow, the velocity term in the non-dimensional analysis of  
 166 the momentum equation is modified to account for external flow,  $\mathbf{u}_{ext}$ , while in the previous

167 definitions (Eq. (9)), the velocity term was non-dimensionalized by the drift velocity of  
 168 charges  $u_{drift} = \mu_b \Delta \phi_0 / H$ . Here, we consider the velocity of the upper wall  $\mathbf{u}_{ext} = u_{wall} \mathbf{e}_x$  in  
 169 Couette flow or the centerline velocity  $\mathbf{u}_{ext} = u_{center} \mathbf{e}_x$  for Poiseuille flow, where  $\mathbf{e}_x$  is the x-  
 170 direction unit vector. For a system with the cross-flow the governing equations become:

$$171 \quad \nabla^* \square \mathbf{u}^* = 0, \quad (10)$$

$$172 \quad \frac{D^* \mathbf{u}^*}{Dt^*} = -\nabla^* P^* + \frac{1}{Re} \nabla^{*2} \mathbf{u}^* - X \rho_c^* \nabla^* \phi^* + \frac{H}{\rho |\mathbf{u}_{ext}|^2} F_p, \quad (11)$$

$$173 \quad \frac{\partial^* \rho_c^*}{\partial t^*} + \nabla^* \square \left[ (u_{ext}^* \mathbf{u}^* - \nabla^* \phi^*) \rho_c^* - \frac{1}{Fe} \nabla^* \rho_c^* \right] = 0, \quad (12)$$

$$174 \quad \nabla^{*2} \phi^* = -C \rho_c^*, \quad (13)$$

175 where  $Re = \frac{\rho |\mathbf{u}_{ext}| H}{\mu}$  - Reynolds number,  $X = \frac{\rho_0 \Delta \phi_0}{\rho |\mathbf{u}_{ext}|^2}$  - a ratio of electric force to inertial  
 176 force [68],  $u_{ext}^* = |\mathbf{u}_{ext}| / u_{drift}$  - the non-dimensional external velocity, and  $F_p$  is a uniform force  
 177 for Poiseuille cross-flow and zero otherwise, such that  $u_{center} = \frac{1}{2\mu} \left( \frac{H}{2} \right)^2 F_p$ . Although X  
 178 was first introduced to analyze the local flow acceleration effect due to electric force [68], the  
 179 parameter can also be used in global stability analysis by adopting the global variables  
 180 ( $\rho_0$  and  $\Delta \phi_0$ ), which has a direct analogy to Richardson number in flow with heat convection  
 181 (Ri - ratio of buoyancy to viscous shear) [59,60,70].

### 182 III. RESULT AND DISCUSSION

183 The TRT LBM approach is used to solve the transport equations for fluid flow and  
 184 charge density, coupled to a fast Poisson solver for electric potential [65]. The equilibrium  
 185 state was obtained when the flow patterns became stable. The numerical code is in SI units,  
 186 and the physical constants are determined by the non-dimensional parameters. The numerical  
 187 method is implemented in C++ using CUDA GPU computing. The number of threads in the  
 188 x-direction in each GPU block is equal to  $NX$ ; the number of GPU blocks in the y-direction  
 189 is equal to  $NY$ . FFT and IFFT operations are performed using the cuFFT library [71]. All  
 190 variables are computed with double precision to reduce truncation errors. The numerical  
 191 method was shown to be 2<sup>nd</sup> order accurate in space. Error analysis is provided in  
 192 supplementary materials [72]. To reduce computational cost while maintaining accuracy, the  
 193 grid of  $NX = 122$ ,  $NY = 100$  is used throughout this work. The macroscopic and mesoscopic  
 194 boundary conditions are specified in **Table I**. The no-slip boundary conditions are applied at  
 195 both electrodes for fluid flow. A constant charge density at the anode (lower wall) represents  
 196 a unipolar injection; a zero-diffusive flux condition  $\nabla \rho_c = 0$  at the cathode (upper wall)  
 197 represents an outflow current. A constant electric potential is applied at the anode; the  
 198 cathode is grounded ( $\phi = 0$ ). At mesoscale, the discrete distribution function of velocity  
 199  $f_i(\mathbf{x}, t)$  and charge density  $g_i(\mathbf{x}, t)$  are used. The details on the transformations between  
 200 macro-variables ( $\mathbf{u}$ ,  $\rho_c$ ) and meso-variables ( $f_i$ ,  $g_i$ ) are presented in the supplementary  
 201 materials [72] and can be found in the recent publication [65]. The LBM full-way bounce-  
 202 back (FBB) scheme is used for the Dirichlet (no-slip) boundary conditions for the fluid flow

203 [19,20,73] and for charge density at the lower wall. The  $g_i$  Neumann boundary condition is  
 204 set as a current outlet boundary condition for charge density transport [19,20,74].

205  
 206

**Table I.** Boundary conditions for the numerical simulations.

Boundary	Macro-variables Conditions	Meso-variables Conditions
x direction	Periodic	Periodic
Upper wall	$\mathbf{u} = 0$ , $\varphi = 0$ and $\nabla \rho_c = 0$	LBM FBB scheme for $f_i$ [74-78] Neumann boundary condition $\frac{\partial g_i}{\partial y} = 0$
Lower wall	$\mathbf{u} = 0$ , $\varphi = \varphi_0$ and $\rho_c = \rho_0$	LBM FBB for $f_i$ [74-78] LBM FBB for $g_i$ [74-78]

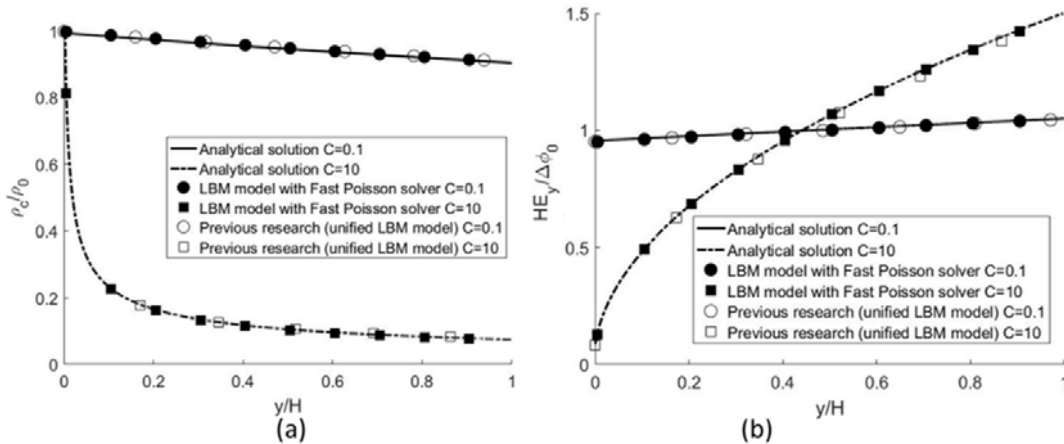
207  
 208  
 209  
 210  
 211

For the hydrostatic based state the numerical solutions of electric field and charge density agree with the model of Luo et al. [19,20] and the analytical solution based on a reduced set of equations for the electric field in 1D coordinates [61,69], see FIG. 1. This comparison acts as a validation of the numerical method.

212 
$$\rho_c = \rho_a (y + y_a)^{-1/2}, \quad (14)$$

213 
$$E_y = \frac{2\rho_a}{\epsilon} (y + y_a)^{1/2}, \quad (15)$$

214 where  $\rho_a$  and  $y_a$  are two-dimensional parameters, which depend on the boundary conditions  
 215 and geometry. At the hydrostatic based state, parameter  $C$  and  $Fe$  dominates the system. FIG.  
 216 1 shows the profiles of normalized charge density and electric field for  $C = 0.1$  and  
 217  $C = 10$  with  $Fe = 4000$ . A more detailed description of the analytical solution is included in  
 218 the supplementary material [72].



219  
 220  
 221  
 222

**FIG. 1.** Hydrostatic solution comparison of the TRT LBM and fast Poisson solver[65], unified SRT LBM [19], and the analytical solution [61,69] for  $C = 0.1$  and  $C = 10$ ,  $Fe = 4000$ . (a) Electric field and (b) charge density.

223  
 224

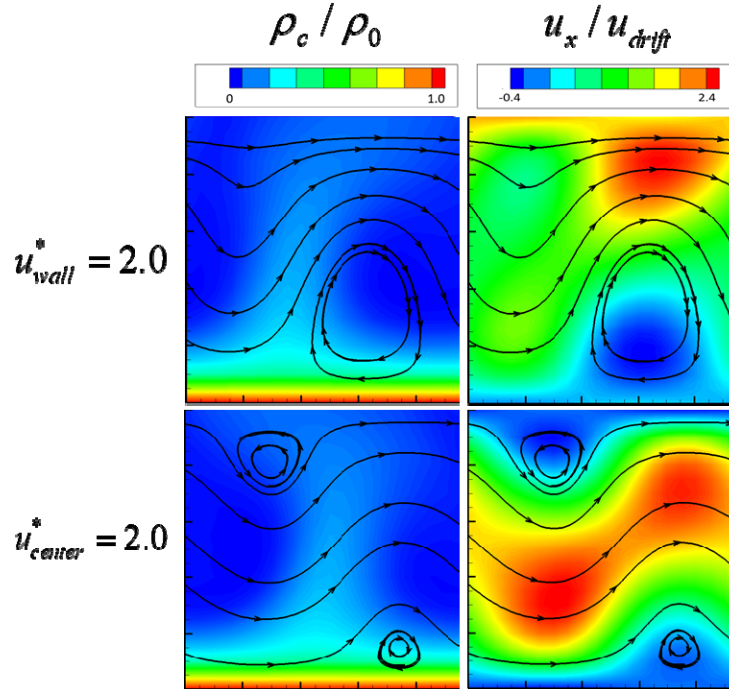
To model EC vortices, the hydrostatic base-state is perturbed using a finite-amplitude wave-form functions that satisfies the boundary conditions and continuity equation:

$$\begin{aligned}
u_x &= L_x \sin(2\pi y / L_y) \sin(2\pi x / L_x) \times \varepsilon \\
u_y &= L_y \left[ \cos(2\pi y / L_y) - 1 \right] \cos(2\pi x / L_x) \times \varepsilon
\end{aligned}
\tag{16}$$

225  
226

227 The physical domain size  $L_x=1.22m$  and  $L_y=1m$  limits the perturbation  
228 wavenumber to  $\lambda_x=2\pi/L_x \approx 5.15(1/m)$ , yielding the most unstable mode under the  
229 conditions  $C=10, M=10$ , and  $Fe=4000$  [20]. The perturbation magnitude,  $\varepsilon=10^{-3}$ , is  
230 small enough to not affect the flow structures within the linear growth region [65]. The  
231 electric Nusselt number,  $Ne=I/I_0$ , serves as a flow stability criteria, where  $I$  is the  
232 cathode current for a given solution and  $I_0$  is the cathode current for the hydrostatic solution  
233 [9,20]; thus if the EC vortices exist,  $Ne>1$ . In the cases with strong ion injection, the EC  
234 stability largely depends on  $T$ ; so, in this analysis,  $T$  is varied while other non-dimensional  
235 parameters are held constant at  $C=10$ ,  $M=10$ , and  $Fe=4000$ .

236 Couette cross-flow is added to the simulation with the established EC vortices by  
237 assigning constant upper wall velocity. To model Poiseuille flow, a body force in the x-  
238 direction is added. FIG. 2 shows the charge density and x-direction velocity for intermediate  
239 cross-flow strength Couette cross-flow ( $u_{wall}^* = 2.0$ ) and Poiseuille cross-flow ( $u_{center}^* = 2.0$ ) at  
240  $T=170.07$ . The Couette cross-flow stretches the vortices in the direction of the bulk flow,  
241 eliminating one of the two vortices. In a Poiseuille cross-flow, the vortex pair becomes  
242 separated; the vortices are pushed toward the opposite walls. With the increasing cross-flow,  
243 both vortices are eliminated, and  $I=I_0$ ,  $Ne=1$  (see FIG. 6). The EC contribution to the flow  
244 field is negligible at higher values of shear stress (higher velocity), and the flow field  
245 becomes identical to the cross-flow without the charge injection.

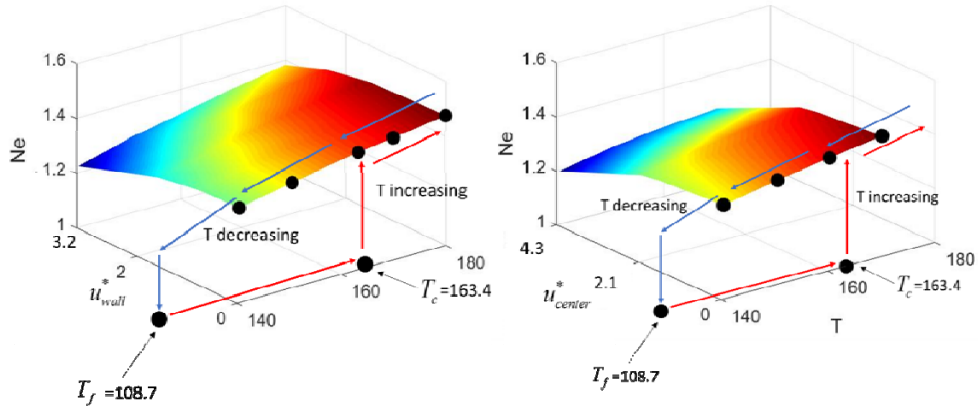


246



247 **FIG. 2.** Charge density and x-direction velocity color contours of the EC with cross-flow. Top:  
 248 Couette flow with  $u_{wall}^* = 2.0$ ; one of the two vortices is suppressed. Bottom: Poiseuille flow with  
 249  $u_{center}^* = 2.0$ ; both vortices are suppressed and displaced towards the walls.

250 FIG. 3 shows the extended stability analysis of EC without cross-flow [65] by  
 251 introducing (a) finite velocity of the upper wall (cathode) and (b) a uniform body force for  
 252 pressure-driven flow  $F_p$ . For a constant  $T$ ,  $Ne$  decreases as  $u_{wall}^*$  or  $u_{center}^*$  increases. **FIG. 3**  
 253 shows that in the cases without cross-flow, a hysteresis loop is observed for  $Ne$  as a function  
 254 of  $T$ , which is consistent with previous theoretical studies [13,18], experimental results [46],  
 255 and numerical simulations [11,15,17,19,20,65]. The shape of the  $Ne$  vs.  $T$  plot in cases with  
 256 cross-flow is similar. However, the magnitude of  $Ne$  is lower, thus the convective charge  
 257 transport (and the current) are reduced when the crossflow is applied due to the partial  
 258 suppression of the EC vortices.



259 **FIG. 3.** Electric Nusselt number as a function of the electric Rayleigh number  $T$  and (a) applied  
 260 velocity of the upper wall  $u_{wall}^*$  for Couette type cross-flow or (b) applied body force  $F_p$  represented  
 261 by the centerline velocity  $u_{center}^*$  for Poiseuille type cross-flow. Partial suppression of the EC vortices  
 262 leads to the reduction in electroconvection for the entire range of the electric Rayleigh number.  
 263

264 FIG. 4 (a-b) shows that  $Ne$  decreases as  $Re$  increases (stronger cross-flow), which  
 265 agrees with the observation that cross-flow suppresses EC vortices and stabilizes the system.  
 266 As previously shown, the intensity of convection strongly depends on  $T$  when cross-flow is  
 267 not present [65]. FIG. 3 shows that when cross-flow is present and while holding  $C$ ,  $M$ , and  
 268  $Fe$  constant,  $Ne = f_1(T, u_{ext}^*)$ . To gain insight into the vortices and the cross-flow interaction,  
 269 it is convenient to plot  $Ne$  vs. non-dimensional groups that contain the velocity term. The  
 270 analysis can be aided by taking a non-dimensional curl ( $\nabla^* \times$ ) of Eq. (6) for  $u_{ext}^* = 0$  and Eq.  
 271 (11) for  $u_{ext}^* \neq 0$ :

$$272 \quad \frac{D^* \omega^*}{D^* t^*} = \frac{M^2}{T} \nabla^{*2} \omega^* - CM^2 (\nabla^* \rho_c^* \times \nabla^* \phi^*), \quad (17)$$

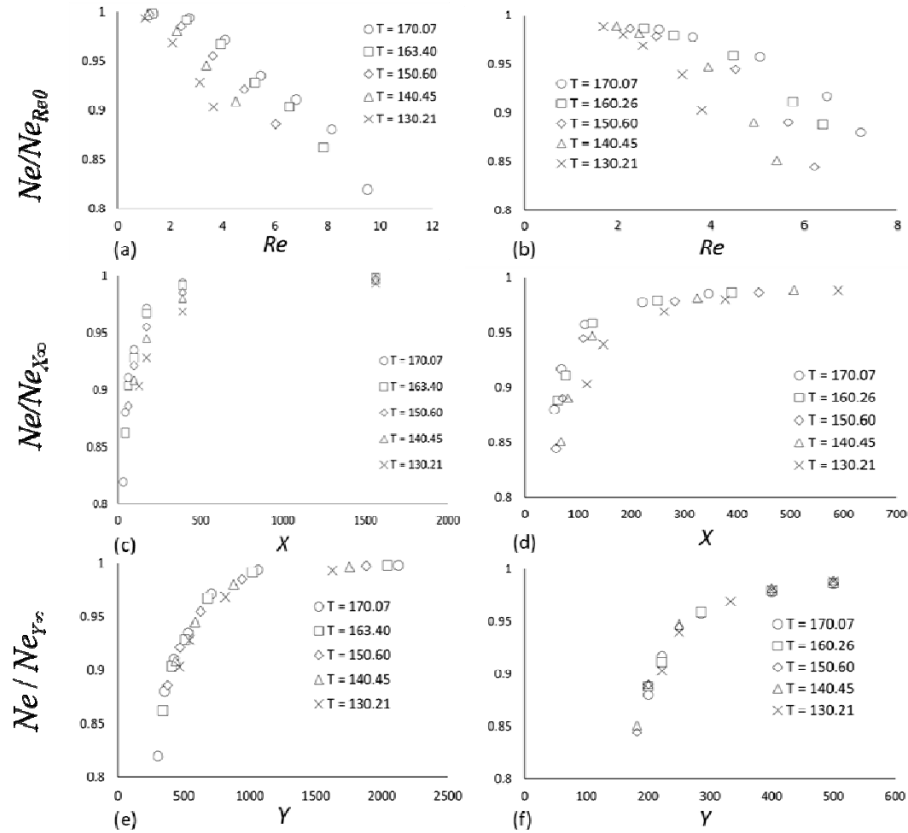
$$273 \quad \frac{D^* \omega^*}{D^* t^*} = \frac{1}{Re} \nabla^{*2} \omega^* - X (\nabla^* \rho_c^* \times \nabla^* \phi^*), \quad (18)$$

274 where  $\omega^*$  is the non-dimensional vorticity, which is a scalar in the 2D flow. The two terms  
 275 on the right-hand side of Eq. (17) and Eq. (18) are significant with respect to growth or decay  
 276 of the vortices. FIG. 4 (a-d) shows that  $Re$  and  $X$  cannot serve as a similarity parameter that

277 describes the behavior of the system. However, if the  $Ne$  plotted against the product of  $Re$  and  
 278  $X$  (defined as  $Y$ ) the  $Ne = f_1(T, u_{ext}^*)$  collapses on a single curve, see FIG. 4 (e-f). Here  $Ne$   
 279 normalized by  $Ne_{Re0}$ ,  $Ne_{X\infty}$  or  $Ne_{Y\infty}$ , which are the solutions without cross-flow  
 280  $Re \rightarrow 0, X \rightarrow \infty, Y \rightarrow \infty$  [65]. The physical interpretation of  $Y$  is as follows. Since  $Re$  is the  
 281 ratio of inertia to viscous force and  $X$  is the ratio of electric force to inertia, their product is  
 282 the ratio of electric force to viscous force:

$$283 \quad Y = X \times Re = \frac{\rho_0 \Delta \phi_0 H}{\mu |u_{ext}|} = \frac{\rho_0 \Delta \phi_0}{|\tau|}, \quad (19)$$

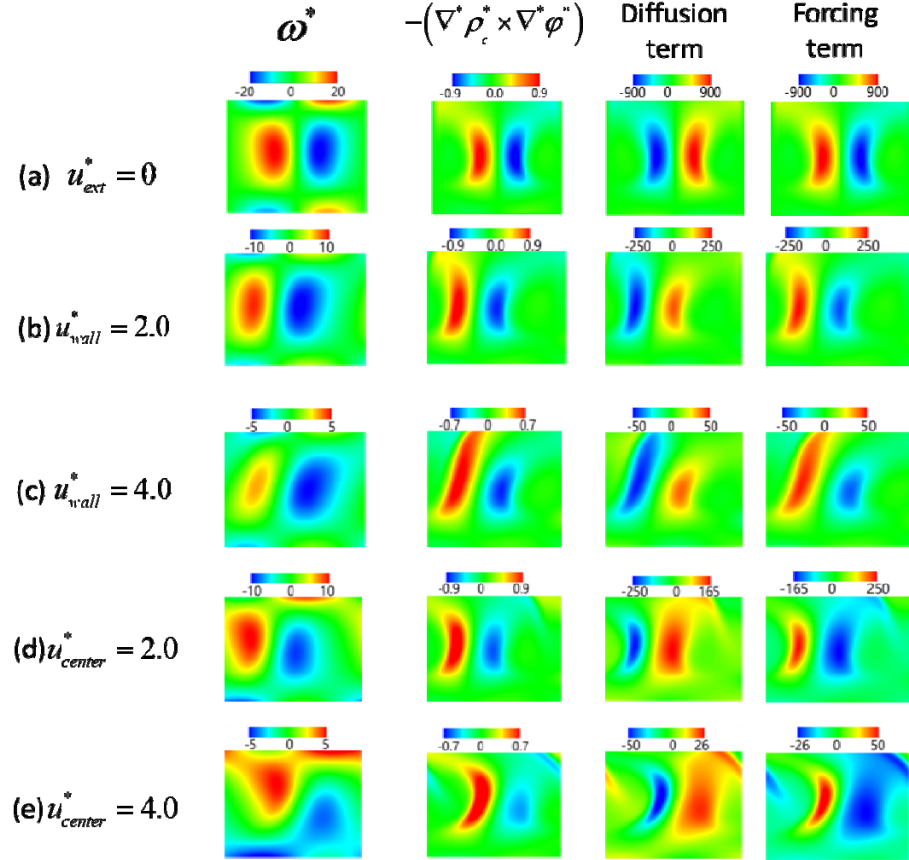
284 where  $\tau$  is the shear stress. In Couette flow,  $\tau = constant$ ; in Poiseuille flow, the average  
 285 value for the channel flow is used. In terms of non-dimensional parameters  $M, C, T$ , and  $u_{ext}^*$ ,  
 286  $X = CM^2 / (u_{ext}^*)^2$  and  $Y = CT / u_{ext}^*$ . When the cross-flow is not  
 287 present,  $Ne_{Re0} = Ne_{X\infty} = Ne_{Y\infty} = f_2(T)$  [19,20,65]. Since  $Ne / Ne_{Y\infty}(T)$  collapse on the same  
 288 curve when plotted against  $Y$ , the EC stability in cross-flow can be parameterized by a single  
 289 non-dimensional parameter, which is inversely proportional to  $\tau$ . In other words,  
 290  $Ne / Ne_{Y\infty} = f_1(T, u_{ext}^*) / f_2(T) = f_3(T / u_{ext}^*)$  for constant  $C, M$ , and  $Fe$ , ( $f_i(\square), i=1,2,3$  denotes  
 291 a functions of). As the  $Y = CT / u_{ext}^*$  for  $C=const$ ,  $Ne / Ne_{Y\infty} = f_3(T / u_{ext}^*) = f_3(Y)$ . **FIG. 4**  
 292 shows the solutions with the established EC vortices, which represents the upper bifurcation  
 293 branch with  $Ne > 1$  (as shown in **FIG. 6**).



295 **FIG. 4.** Electric Nusselt vs. non-dimensional parameters. (a,c,e) Couette cross-flow is applied. (b,d,f)  
 296 Poiseuille type cross-flow is applied. (a-b) The  $Ne/Ne_{Re0}$  vs.  $Re$  showing that the flow becomes more  
 297 stable for increasing  $Re$  or cross-flow. (c-d) The  $Ne/Ne_{X\infty}$  vs.  $X$ . (e-f) The  $Ne/Ne_{Y\infty}$  collapses on a  
 298 single curve for various  $T$  and  $Y$  indicating that  $Ne/Ne_{Y\infty}$  is only a function of  $Y$  for constant  $C$ .  $Ne_{Re0} =$   
 299  $Ne_{X\infty} = Ne_{Y\infty}$  is the electric Nusselt number without cross-flow

300 **FIG. 5** shows the effects of intermediate and strong cross-flow on vorticity  $\omega^*$  and curl  
 301 of electric force  $-(\nabla^* \rho_c^* \times \nabla^* \phi^*)$ , the diffusion term  $\frac{M^2}{T} \nabla^{*2} \omega^*$  as in Eq. (17) without cross-  
 302 flow or  $\frac{1}{Re} \nabla^{*2} \omega^*$  as in Eq. (18) with cross-flow, and the forcing term  $-CM^2 (\nabla^* \rho_c^* \times \nabla^* \phi^*)$  as in  
 303 Eq. (17) without cross-flow or  $-X (\nabla^* \rho_c^* \times \nabla^* \phi^*)$  as in Eq. (18) with cross-flow. As expected,  
 304 maximum and minimum values of vorticity correlate with the maximum and minimum values  
 305 of the curl of electric force and forcing term, see Eq. (17) and Eq. (18), implying that  
 306 coulombic forcing term leads to vorticity generation. When an intermediate cross-flow is  
 307 applied (**FIG. 5** (b,d)), the symmetry of the vortex pair is disrupted, and the curl of the  
 308 electric force is also asymmetric. For strong cross-flow (**FIG. 5** (c,e)), the magnitudes forcing  
 309 term is lower, leading to lower vorticity generation. One of the most significant findings in  
 310 this analysis is that the reduction in the forcing term  $X (\nabla^* \rho_c^* \times \nabla^* \phi^*)$  does not come from the  
 311 expression  $(\nabla^* \rho_c^* \times \nabla^* \phi^*)$  but rather from the  $X$ , as seen by comparing **FIG. 5** (columns 2 and  
 312 4). Thus variations in values of  $X$  are responsible for the changes in vorticity generation.

313 On the other hand, it is apparent from **FIG. 5** the diffusion balances the forcing term; for  
 314 all the cases, the diffusion terms have equal and opposite values of the forcing terms over the  
 315 wide range of values, while the vorticity magnitudes do not change significantly. Similarly to  
 316 the forcing, the diffusion term in Eq. (18) is the product of two non-dimensional groups:  $1/Re$   
 317 and  $\nabla^{*2} \omega^*$ . **FIG. 4** shows that  $Re$  changes by order of magnitude acting as a scaling factor in  
 318 the diffusion term Eq. (18). Multiplication of both diffusion and forcing terms by  $Re$  yields a  
 319 coefficient of unity in diffusion term and parameter  $Y$  in the forcing term.



320

321 **FIG. 5.** Color contours of vorticity  $\omega^*$ , curl of electric force  $-(\nabla^* \rho_c^* \times \nabla^* \phi^*)$ , diffusion and forcing  
 322 terms from Eq. (17) and Eq. (18) with and without cross-flow. (a): No cross-flow; both vortices exist  
 323 (b): Intermediate Couette flow with  $u_{wall}^* = 2.0$ ; one of the two vortices is suppressed. (c): Strong  
 324 Couette flow with  $u_{wall}^* = 4.0$ . (d): Intermediate Poiseuille flow  $u_{center}^* = 2.0$ ; vortices are suppressed  
 325 and displaced towards the walls. (e): Strong Poiseuille flow with  $u_{center}^* = 4.0$ .

326 To examine hysteresis associated with the formation and suppression of EC vortices, FIG.  
 327 6 shows the  $Ne = f(Y)$  for fixed  $C = 10$ ,  $M = 10$ ,  $T = 170.07$ , and  $Fe = 4000$ . Both Couette  
 328 and Poiseuille cross-flow are examined. A hysteresis loop with subcritical bifurcation is  
 329 observed; the bifurcation thresholds are  $Y_c = 625.25$ ,  $Y_f = 297.32$  for Couette flow and  
 330  $Y_c = 218.58$ ,  $Y_f = 159.36$  for Poiseuille flow. The critical values of  $Y_c$  correspond to  $Re_c \sim O(1)$   
 331 ( $Re_c = 4.63$  for Couette flow and  $Re_c = 2.94$  for Poiseuille flow), which is consistent with linear  
 332 stability analysis [64] for  $T = 170.07$ . Similar to stability parameter  $T$  for  $Re = 0$  (FIG. 3), for  
 333  $Y < Y_c$ , the system does not yield the EC instability, returning to the unperturbed state  
 334 ( $I = I_0$  and  $Ne = 1$ ). If  $Y$  decreases after the EC vortices are formed,  $Ne$  decreases  
 335 nonlinearly, until  $Y = Y_f$ , then the EC vortices are suppressed; the flow is not influenced by  
 336 the electric forces.

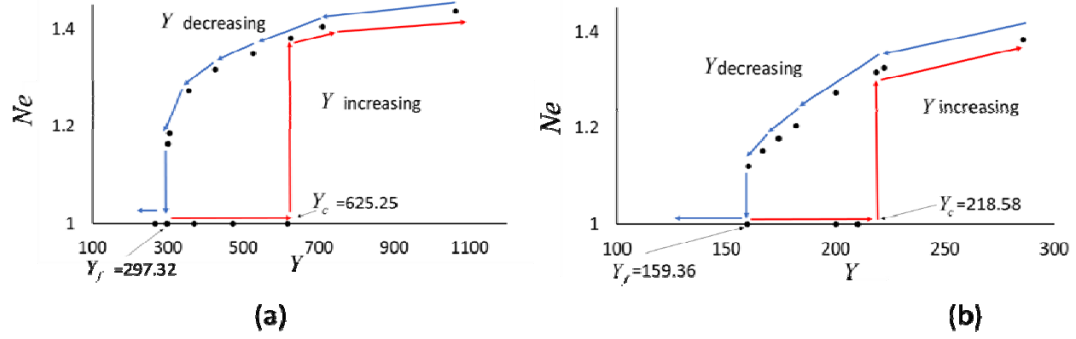


**FIG. 6.** Electrical Nusselt number  $Ne$  versus  $Y$ . Bifurcation thresholds are: (a) Couette cross-flow  $Y_c = 625.25$  and  $Y_f = 297.32$ ; (b) Poiseuille cross-flow  $Y_c = 218.58$  and  $Y_f = 159.36$ .

The results presented in this work consider the interaction crossflow electroconvective transport due to the unipolar charge injection; the presented methodology can be extended to more complex convective systems such as RBC and charge-neutral electrokinetic systems. The 2D case in this work can be regarded as a special case in the 3D flow scenario, i.e., the traverse rolling pattern [19,20]. Multimodal 3D structures (square patterns, hexagonal patterns, and mixed patterns) are ubiquitous in convective flows such as in EKI [58], EHD [20,21,79], and RBC[51,52,59,80-83]. The effect of cross-flow has been observed in all three scenarios; the summary and the analogy to EKI and RBC is shown in **Table II**.

**Table II.** Non-dimensional parameters analogy for RBC and EHD electroconvection in the presence of the cross-flow velocity  $\mathbf{u}_{ext}$

Physical interpretation	Electrohydrodynamic convection (EHD)		Heat convection (RBC)
	As presented here (including charge density)	Based on average field properties (without charge density)	
$\frac{\text{Body force}}{\text{inertial force}}$	$X = \frac{\rho_0 \Delta \phi_0}{\rho  \mathbf{u}_{ext} ^2}$ [68]	$N_{ei} = \frac{\epsilon \Delta \phi_0^2}{\rho H^2  \mathbf{u}_{ext} ^2}$ [84,85]	$Ri = Gr / Re^2 = \frac{g' H}{ \mathbf{u}_{ext} ^2}$ [59]
$\frac{\text{Body force}}{\text{viscous force}}$	$Y = X \times Re = \frac{\rho_0 \Delta \phi_0}{ \boldsymbol{\tau} }$	$N_{ev} = N_{ei} \times Re = \frac{\epsilon \Delta \phi_0^2}{\mu H  \mathbf{u}_{ext} }$ [84,85]	$Gr / Re = \frac{g' \rho H^2}{\mu  \mathbf{u}_{ext} }$

where  $g' = g \frac{\Delta \rho}{\rho}$  is the reduced gravity [60]. In the context of EKI, the convection can also be characterized by non-dimensional parameters such as electric Nusselt number, electric Rayleigh number and Reynolds number [30,31].

#### IV. CONCLUSION

The 2D numerical study extends the EC stability analysis to Couette and Poiseuille flows between two infinitely long parallel electrodes with unipolar charge injection. The numerical approach utilizes the two-relaxation-time LBM to solve the flow and charge transport equations and a Fast Poisson Solver to solve the Poisson equation. Increasing cross-flow velocity deforms the vortices and eventually suppresses them when threshold values of velocities are reached. Partial suppression of the vortices leads to the reduction in electroconvection for the entire range of the electric Rayleigh number. The non-dimensional analysis of the governing equations is used to derive parameter  $Y$ , a ratio of electric force to viscous force, in the presence of cross-flow. The non-dimensional parameter  $Y$  accounts for

363 the effect of the shear stress, analogous to the Richardson number,  $Ri$  - ratio of buoyancy to  
364 the inertial forces, that is used to parametrize the effect of the applied shear in RBC. Similar  
365 to the stability parameter  $T$  for the hydrostatic case, a hysteresis loop with subcritical  
366 bifurcation is observed. For  $C = 10$ ,  $M = 10$ ,  $T = 170.07$ , and  $Fe = 4000$ , the bifurcation  
367 thresholds are  $Y_c = 625.25$ ,  $Y_f = 297.32$  for Couette flow and  $Y_c = 218.58$ ,  $Y_f = 159.36$  for  
368 Poiseuille flow.

369

## V. ACKNOWLEDGMENTS

370 This research was supported by the DHS Science and Technology Directorate and UK Home  
371 Office, grant no. HSHQDC-15-531 C-B0033 and by the National Institutes of Health, grant  
372 no. NIBIB U01 EB021923.

373

## VI. REFERENCES

- 374 [1] G. I. Taylor, Studies in electrohydrodynamics. I. The circulation produced in a drop  
375 by an electric field, Proceedings of the Royal Society of London. Series A. Mathematical and  
376 Physical Sciences **291**, 159 (1966).
- 377 [2] D. C. Jolly and J. R. Melcher, Electroconvective instability in a fluid layer,  
378 Proceedings of the Royal Society of London. A. Mathematical and Physical Sciences **314**,  
379 269 (1970).
- 380 [3] B. Malraison and P. Atten, Chaotic behavior of instability due to unipolar ion  
381 injection in a dielectric liquid, Physical Review Letters **49**, 723 (1982).
- 382 [4] A. Castellanos and P. Atten, Numerical modeling of finite amplitude convection of  
383 liquids subjected to unipolar injection, IEEE transactions on industry applications, 825  
384 (1987).
- 385 [5] Z. A. Daya, V. B. Deyirmenjian, and S. W. Morris, Bifurcations in annular  
386 electroconvection with an imposed shear, Physical Review E **64**, 036212 (2001).
- 387 [6] K. Adamiak and P. Atten, Simulation of corona discharge in point-plane  
388 configuration, Journal of electrostatics **61**, 85 (2004).
- 389 [7] P. Tsai, Z. A. Daya, and S. W. Morris, Aspect-ratio dependence of charge transport in  
390 turbulent electroconvection, Physical review letters **92**, 084503 (2004).
- 391 [8] P. Tsai, Z. A. Daya, and S. W. Morris, Charge transport scaling in turbulent  
392 electroconvection, Physical Review E **72**, 046311 (2005).
- 393 [9] P. Traoré and A. Pérez, Two-dimensional numerical analysis of electroconvection in a  
394 dielectric liquid subjected to strong unipolar injection, Physics of Fluids **24**, 037102 (2012).
- 395 [10] P. Traoré and J. Wu, On the limitation of imposed velocity field strategy for  
396 Coulomb-driven electroconvection flow simulations, Journal of Fluid Mechanics **727** (2013).
- 397 [11] J. Wu, P. Traoré, P. A. Vázquez, and A. T. Pérez, Onset of convection in a finite two-  
398 dimensional container due to unipolar injection of ions, Physical Review E **88**, 053018  
399 (2013).
- 400 [12] A. Pérez, P. Vázquez, J. Wu, and P. Traoré, Electrohydrodynamic linear stability  
401 analysis of dielectric liquids subjected to unipolar injection in a rectangular enclosure with  
402 rigid sidewalls, Journal of Fluid Mechanics **758**, 586 (2014).
- 403 [13] M. Zhang, F. Martinelli, J. Wu, P. J. Schmid, and M. Quadrio, Modal and non-modal  
404 stability analysis of electrohydrodynamic flow with and without cross-flow, Journal of Fluid  
405 Mechanics **770**, 319 (2015).
- 406 [14] P. Traore, J. Wu, C. Louste, P. A. Vazquez, and A. T. Perez, Numerical study of a  
407 plane poiseuille channel flow of a dielectric liquid subjected to unipolar injection, IEEE  
408 Transactions on Dielectrics and Electrical Insulation **22**, 2779 (2015).

- 409 [15] J. Wu and P. Traoré, A finite-volume method for electro-thermoconvective  
410 phenomena in a plane layer of dielectric liquid, *Numerical Heat Transfer, Part A:  
411 Applications* **68**, 471 (2015).
- 412 [16] J. Wu, A. T. Perez, P. Traore, and P. A. Vazquez, Complex flow patterns at the onset  
413 of annular electroconvection in a dielectric liquid subjected to an arbitrary unipolar injection,  
414 *IEEE Transactions on Dielectrics and Electrical Insulation* **22**, 2637 (2015).
- 415 [17] J. Wu, P. Traoré, A. T. Pérez, and P. A. Vázquez, On two-dimensional finite  
416 amplitude electro-convection in a dielectric liquid induced by a strong unipolar injection,  
417 *Journal of Electrostatics* **74**, 85 (2015).
- 418 [18] M. Zhang, Weakly nonlinear stability analysis of subcritical electrohydrodynamic  
419 flow subject to strong unipolar injection, *Journal of Fluid Mechanics* **792**, 328 (2016).
- 420 [19] K. Luo, J. Wu, H.-L. Yi, and H.-P. Tan, Lattice Boltzmann model for Coulomb-  
421 driven flows in dielectric liquids, *Physical Review E* **93**, 023309 (2016).
- 422 [20] K. Luo, J. Wu, H.-L. Yi, and H.-P. Tan, Three-dimensional finite amplitude  
423 electroconvection in dielectric liquids, *Physics of Fluids* **30**, 023602 (2018).
- 424 [21] K. Luo, J. Wu, H.-L. Yi, L.-H. Liu, and H.-P. Tan, Hexagonal convection patterns and  
425 their evolutionary scenarios in electroconvection induced by a strong unipolar injection,  
426 *Physical Review Fluids* **3**, 053702 (2018).
- 427 [22] K. Luo, T.-F. Li, J. Wu, H.-L. Yi, and H.-P. Tan, Mesoscopic simulation of  
428 electrohydrodynamic effects on laminar natural convection of a dielectric liquid in a cubic  
429 cavity, *Physics of Fluids* **30**, 103601 (2018).
- 430 [23] M. Z. Bazant, Electrokinetics meets electrohydrodynamics, *Journal of Fluid  
431 Mechanics* **782**, 1 (2015).
- 432 [24] Y. Mori and Y.-N. Young, From electrodiffusion theory to the electrohydrodynamics  
433 of leaky dielectrics through the weak electrolyte limit, *Journal of Fluid Mechanics* **855**, 67  
434 (2018).
- 435 [25] I. Rubinstein and B. Zaltzman, Electro-osmotically induced convection at a  
436 permselective membrane, *Physical Review E* **62**, 2238 (2000).
- 437 [26] I. Rubinstein and B. Zaltzman, Electro-osmotic slip of the second kind and instability  
438 in concentration polarization at electro dialysis membranes, *Mathematical Models and  
439 Methods in Applied Sciences* **11**, 263 (2001).
- 440 [27] B. Zaltzman and I. Rubinstein, Electro-osmotic slip and electroconvective instability,  
441 *Journal of Fluid Mechanics* **579**, 173 (2007).
- 442 [28] S. M. Rubinstein, G. Manukyan, A. Staicu, I. Rubinstein, B. Zaltzman, R. G.  
443 Lammertink, F. Mugele, and M. Wessling, Direct observation of a nonequilibrium electro-  
444 osmotic instability, *Physical review letters* **101**, 236101 (2008).
- 445 [29] V. S. Pham, Z. Li, K. M. Lim, J. K. White, and J. Han, Direct numerical simulation of  
446 electroconvective instability and hysteretic current-voltage response of a permselective  
447 membrane, *Physical Review E* **86**, 046310 (2012).
- 448 [30] R. Kwak, V. S. Pham, K. M. Lim, and J. Han, Shear flow of an electrically charged  
449 fluid by ion concentration polarization: scaling laws for electroconvective vortices, *Physical  
450 review letters* **110**, 114501 (2013).
- 451 [31] R. Kwak, V. S. Pham, and J. Han, Sheltering the perturbed vortical layer of  
452 electroconvection under shear flow, *Journal of Fluid Mechanics* **813**, 799 (2017).
- 453 [32] C. Druzgalski, M. Andersen, and A. Mani, Direct numerical simulation of  
454 electroconvective instability and hydrodynamic chaos near an ion-selective surface, *Physics  
455 of Fluids* **25**, 110804 (2013).
- 456 [33] S. M. Davidson, M. B. Andersen, and A. Mani, Chaotic induced-charge electro-  
457 osmosis, *Physical review letters* **112**, 128302 (2014).

- 458 [34] S. M. Davidson, M. Wessling, and A. Mani, On the dynamical regimes of pattern-  
459 accelerated electroconvection, *Scientific reports* **6**, 22505 (2016).
- 460 [35] I. Rubinstein and B. Zaltzman, Convective diffusive mixing in concentration  
461 polarization: from Taylor dispersion to surface convection, *Journal of Fluid Mechanics* **728**,  
462 239 (2013).
- 463 [36] I. Rubinstein and B. Zaltzman, Equilibrium electroconvective instability, *Physical*  
464 *review letters* **114**, 114502 (2015).
- 465 [37] D. Saville, Electrohydrodynamics: the Taylor-Melcher leaky dielectric model, *Annual*  
466 *review of fluid mechanics* **29**, 27 (1997).
- 467 [38] P. Watson, J. Schneider, and H. Till, Electrohydrodynamic Stability of Space -  
468 Charge - Limited Currents in Dielectric Liquids. II. Experimental Study, *The Physics of*  
469 *Fluids* **13**, 1955 (1970).
- 470 [39] K. Luo, A. T. Pérez, J. Wu, H.-L. Yi, and H.-P. Tan, Efficient lattice Boltzmann  
471 method for electrohydrodynamic solid-liquid phase change, *Physical Review E* **100**, 013306  
472 (2019).
- 473 [40] K. Luo, J. Wu, A. T. Pérez, H.-L. Yi, and H.-P. Tan, Stability analysis of  
474 electroconvection with a solid-liquid interface via the lattice Boltzmann method, *Physical*  
475 *Review Fluids* **4**, 083702 (2019).
- 476 [41] P. Atten, F. McCluskey, and A. Perez, Electroconvection and its effect on heat  
477 transfer, *IEEE Transactions on Electrical Insulation* **23**, 659 (1988).
- 478 [42] N. Felici, Phénomènes hydro et aérodynamiques dans la conduction des diélectriques  
479 fluides, *Rev. Gén. Electr.* **78**, 717 (1969).
- 480 [43] N. Felici and J. Lacroix, Electroconvection in insulating liquids with special reference  
481 to uni-and bi-polar injection: a review of the research work at the CNRS Laboratory for  
482 Electrostatics, Grenoble 1969–1976, *Journal of Electrostatics* **5**, 135 (1978).
- 483 [44] J. Schneider and P. Watson, Electrohydrodynamic Stability of Space - Charge -  
484 Limited Currents in Dielectric Liquids. I. Theoretical Study, *The Physics of Fluids* **13**, 1948  
485 (1970).
- 486 [45] P. Atten and R. Moreau, Stabilité électrohydrodynamique des liquides isolants soumis  
487 à une injection unipolaire, *J. Mécanique* **11**, 471 (1972).
- 488 [46] P. Atten and J. Lacroix, Non-linear hydrodynamic stability of liquids subjected to  
489 unipolar injection, *Journal de Mécanique* **18**, 469 (1979).
- 490 [47] J. Lacroix, P. Atten, and E. Hopfinger, Electro-convection in a dielectric liquid layer  
491 subjected to unipolar injection, *Journal of Fluid Mechanics* **69**, 539 (1975).
- 492 [48] P. Atten, Rôle de la diffusion dans le problème de la stabilité hydrodynamique d'un  
493 liquide diélectrique soumis à une injection unipolaire forte, *CR Acad. Sci. Paris* **283**, 29  
494 (1976).
- 495 [49] F. Li, B.-F. Wang, Z.-H. Wan, J. Wu, and M. Zhang, Absolute and convective  
496 instabilities in electrohydrodynamic flow subjected to a Poiseuille flow: a linear analysis,  
497 *Journal of Fluid Mechanics* **862**, 816 (2019).
- 498 [50] E. Demekhin, V. Shelistov, and S. Polyanskikh, Linear and nonlinear evolution and  
499 diffusion layer selection in electrokinetic instability, *Physical Review E* **84**, 036318 (2011).
- 500 [51] S. Chandrasekhar, *Hydrodynamic and hydromagnetic stability* (Courier Corporation,  
501 2013).
- 502 [52] P. G. Drazin and W. H. Reid, *Hydrodynamic stability* (Cambridge university press,  
503 2004).
- 504 [53] E. L. Koschmieder, *Bénard cells and Taylor vortices* (Cambridge University Press,  
505 1993).
- 506 [54] P. Bergé and M. Dubois, Rayleigh-bénard convection, *Contemporary Physics* **25**, 535  
507 (1984).



508 [55] M. Krishnan, V. M. Ugaz, and M. A. Burns, PCR in a Rayleigh-Benard convection  
509 cell, *Science* **298**, 793 (2002).

510 [56] A. V. Getling, *Rayleigh-Benard Convection: Structures and Dynamics* (World  
511 Scientific, 1998), Vol. 11.

512 [57] E. Demekhin, N. Nikitin, and V. Shelistov, Direct numerical simulation of  
513 electrokinetic instability and transition to chaotic motion, *Physics of Fluids* **25**, 122001  
514 (2013).

515 [58] E. Demekhin, N. Nikitin, and V. Shelistov, Three-dimensional coherent structures of  
516 electrokinetic instability, *Physical Review E* **90**, 013031 (2014).

517 [59] A. Mohamad and R. Viskanta, Laminar flow and heat transfer in Rayleigh–Benard  
518 convection with shear, *Physics of Fluids A: Fluid Dynamics* **4**, 2131 (1992).

519 [60] J. S. Turner, *Buoyancy effects in fluids* (Cambridge university press, 1979).

520 [61] R. Chicón, A. Castellanos, and E. Martin, Numerical modelling of Coulomb-driven  
521 convection in insulating liquids, *Journal of Fluid Mechanics* **344**, 43 (1997).

522 [62] P. Vazquez, G. Georghiou, and A. Castellanos, Characterization of injection  
523 instabilities in electrohydrodynamics by numerical modelling: comparison of particle in cell  
524 and flux corrected transport methods for electroconvection between two plates, *Journal of*  
525 *Physics D: Applied Physics* **39**, 2754 (2006).

526 [63] A. Castellanos and N. Agrait, Unipolar injection induced instabilities in plane parallel  
527 flows, *IEEE transactions on industry applications* **28**, 513 (1992).

528 [64] J. L. Lara, A. Castellanos, and F. Pontiga, Destabilization of plane Poiseuille flow of  
529 insulating liquids by unipolar charge injection, *Physics of Fluids* **9**, 399 (1997).

530 [65] Y. Guan and I. Novosselov, Two Relaxation Time Lattice Boltzmann Method  
531 Coupled to Fast Fourier Transform Poisson Solver: Application to Electroconvective Flow,  
532 *Journal of Computational Physics* **397**, 108830 (2019).

533 [66] J. Wu, P. Traoré, M. Zhang, A. T. Pérez, and P. A. Vázquez, Charge injection  
534 enhanced natural convection heat transfer in horizontal concentric annuli filled with a  
535 dielectric liquid, *International Journal of Heat and Mass Transfer* **92**, 139 (2016).

536 [67] Y. Zhang, L. Liu, Y. Chen, and J. Ouyang, Characteristics of ionic wind in needle-to-  
537 ring corona discharge, *Journal of Electrostatics* **74**, 15 (2015).

538 [68] Y. Guan, R. S. Vaddi, A. Aliseda, and I. Novosselov, Experimental and numerical  
539 investigation of electrohydrodynamic flow in a point-to-ring corona discharge, *Physical*  
540 *Review Fluids* **3**, 043701 (2018).

541 [69] Y. Guan, R. S. Vaddi, A. Aliseda, and I. Novosselov, Analytical model of electro-  
542 hydrodynamic flow in corona discharge, *Physics of plasmas* **25**, 083507 (2018).

543 [70] H. D. Abarbanel, D. D. Holm, J. E. Marsden, and T. Ratiu, Richardson number  
544 criterion for the nonlinear stability of three-dimensional stratified flow, *Physical Review*  
545 *Letters* **52**, 2352 (1984).

546 [71] N. Goodnight, CUDA/OpenGL fluid simulation, NVIDIA Corporation (2007).

547 [72] Y. Guan and I. Novosselov, See supplemental material for the analytical solutions,  
548 LBM scheme details, and error analysis, *Physical Review Fluids* (2019).

549 [73] I. Ginzbourg and P. Adler, Boundary flow condition analysis for the three-  
550 dimensional lattice Boltzmann model, *Journal de Physique II* **4**, 191 (1994).

551 [74] T. Krüger, H. Kusumaatmaja, A. Kuzmin, O. Shardt, G. Silva, and E. M. Viggien, *The*  
552 *Lattice Boltzmann Method* (Springer, 2017).

553 [75] I. Ginzburg, F. Verhaeghe, and D. d’Humières, Two-relaxation-time lattice  
554 Boltzmann scheme: About parametrization, velocity, pressure and mixed boundary  
555 conditions, *Communications in computational physics* **3**, 427 (2008).

556 [76] S. Khirevich, I. Ginzburg, and U. Tallarek, Coarse-and fine-grid numerical behavior  
557 of MRT/TRT lattice-Boltzmann schemes in regular and random sphere packings, Journal of  
558 Computational Physics **281**, 708 (2015).  
559 [77] I. Ginzburg, L. Roux, and G. Silva, Local boundary reflections in lattice Boltzmann  
560 schemes: Spurious boundary layers and their impact on the velocity, diffusion and dispersion,  
561 Comptes Rendus Mécanique **343**, 518 (2015).  
562 [78] I. Ginzburg, Prediction of the moments in advection-diffusion lattice Boltzmann  
563 method. II. Attenuation of the boundary layers via double- $\Lambda$  bounce-back flux scheme,  
564 Physical Review E **95**, 013305 (2017).  
565 [79] Y. Guan;, J. Riley;, and I. Novosselov;, Three-dimensional Electro-convective  
566 Vortices in Cross-flow, arXiv preprint arXiv:1908.03861 (2019).  
567 [80] H. Müller, M. Lücke, and M. Kamps, Transversal convection patterns in horizontal  
568 shear flow, Physical Review A **45**, 3714 (1992).  
569 [81] H. Müller, M. Lücke, and M. Kamps, Convective patterns in horizontal flow, EPL  
570 (Europhysics Letters) **10**, 451 (1989).  
571 [82] H. Müller, M. Tveitereid, and S. Trainoff, Rayleigh-Bénard problem with imposed  
572 weak through-flow: two coupled Ginzburg-Landau equations, Physical Review E **48**, 263  
573 (1993).  
574 [83] M. Tveitereid and H. W. Müller, Pattern selection at the onset of Rayleigh-Bénard  
575 convection in a horizontal shear flow, Physical Review E **50**, 1219 (1994).  
576 [84] IEEE-DEIS-EHD-Technical-Committee, Recommended international standard for  
577 dimensionless parameters used in electrohydrodynamics, IEEE Transactions on Dielectrics  
578 and Electrical Insulation **10**, 3 (2003).  
579 [85] J.-S. Chang, A. J. Kelly, and J. M. Crowley, *Handbook of electrostatic processes*  
580 (CRC Press, 1995).  
581  
582  
583